Numerical Simulation of the effect of wind gusts on a micro-drone wing / Effects of wing tip vortexes

June 2019

Francís Adrián Meziat Ramírez*, Valérie Ferrand† and Thierry Jardin†
*Institut Supérieur de l'Aéronautique et de l'Espace (ISAE-SUPAERO), Université de Toulouse, 31055 Toulouse, FRANCE
Email: francis-adrian.meziat-ramirez@student.isae-supaero.fr
†Institut Supérieur de l'Aéronautique et de l'Espace (ISAE-SUPAERO), Université de Toulouse, 31055 Toulouse, FRANCE
Email: {valerie.ferrand,thierry.jardin}@isae.fr

***Abstract*—This research project focuses on the numerical study of the unsteady effects of longitudinal wind gusts on the aerodynamic performance of micro-drone wings. The flow structure and the unsteady-to-quasi-steady lift ratio evolution were studied at low Reynolds numbers and reduced frequencies. The applicability and limitations of Greenberg's Theory were assessed in such 2D cases. A series of unsteady Direct Numerical Simulations were performed in order to do so. This showed that viscosity effects are too dominant at the low Reynolds numbers which were possible to simulate through DNS and thus that the unsteady effects observed in the simulations cannot be extrapolated to the experimental high Reynolds number case.**

NOMENCLATURE

α	Angle of attack
Δt	Time-step duration
Δx	Cell size
σ	Surging amplitude
φ	Velocity phase
c	Chord
C_L	Lift coefficient
C_P	Pressure coefficient
D	Drag
f	Surging frequency
f_{VS}	Vortex shedding frequency
k	Reduced frequency
L	Lift
Re	Chord Reynolds number
Re_{cell}	Cell Reynolds number
St	Strouhal number
T	Surging period
t	Time
U	Longitudinal inlet velocity
U_∞	Mean longitudinal free-stream velocity

I. INTRODUCTION

At low altitude, the airflow is strongly unsteady, with turbulent fluctuations extending along a wide variety of spatial and temporal scales. This region is known as the atmospheric boundary layer. Both meteorological conditions and topography are responsible for this phenomenon. For instance, in cities, the wakes produced by buildings represent an important source of unsteadiness for wind conditions. Micro-drones tend to fly at low altitudes in urban areas; moreover, they tend to be lightweight, which makes them very sensitive to atmospheric turbulence and wind gusts, which can have a magnitude comparable to their cruise velocity [6]. Thus, if hit by wind gusts, the effects on the aerodynamic performance of these kinds of aircraft can seriously compromise their mission (image recording, surveillance, item delivery and so on). This study aims to take further the understanding of the complex unsteady mechanisms that aircraft flying at low Reynolds number undergo when entering a longitudinal wind gust.

In order to characterise the stated phenomena, a Direct Numerical Simulation (DNS) Study, using StarCCM+ of a micro-drone type wing (NACA 0012 aerofoil) subject to a near-sinusoidal wind gust was carried out. For high aspect ratio wings, the aerodynamic response to this kind of perturbation is determined by vortex generation at the leading edge of the aerofoil. However, for micro drone wings (with low aspect ratios ranging from 2 to 6), the unsteady behaviour is affected by the interaction of leading-edge vortexes with wingtip vortexes (an example of wingtip vortex visualisation using coloured smoke can be seen in Figure 1). The main problematic in 3D cases is to numerically address the role of the wingtip vortex in the airflow and the generation of unsteady aerodynamic loads. That was the initial goal of the project. However, many issues had to be studied in 2D configurations before moving to 3D. Thus, this research focused on the assessment of the validity of the Direct Numerical Simulation (limited to $Re = 1000$) to correctly predict the unsteady effects and flow structure found in the experimental case (with $Re = 10^5$), in order to set the basis for a future 3D study. This was accomplished through 2D simulations where the results were compared to those granted by Greenberg's Theory [4]. The numerical simulation were validated and its results compared with the experimental data recorded in a project carried out in parallel at ISAE-SUPAERO's Aerodynamics, Energetics and Propulsion Department (DAEP).

Greenberg's Theory [4] can predict the existence of unsteady effects on the aerodynamic loads on an aerofoil. However, it is limited to small amplitude harmonic motions in a pulsating stream of 2D aerofoils at low angles of attack, assuming inviscid flow and such that no flow separation occurs. Thus, many important and complex phenomena are

Fig. 1: Wake Vortex Study at Wallops Island - NASA [3]

overlooked by this theory; in addition the 3D effects are not considered. One of the main interests of this project was to evaluate whether Greenberg's Theory was applicable or not for certain Reynolds, reduced frequencies and amplitudes. Recent works by Strangfeld [5] have experimentally evaluated predictions by the existing theory in the case of a 2D aerofoil in a high amplitude harmonic oscillating stream at constant angle of attack. Their conclusions assess the importance of the separation bubble, specially its position and shedding, which are decisive in the validity of the theoretical predictions. In this case, the 2D experimental configuration does not allow for the study of 3D effects, including wingtip vortexes. Other authors such as Barnes and Visbal [1], [2] have performed numerical studies (high-fidelity implicit large eddy simulations) assessing the unsteady flow structure around NACA 0012 aerofoils subject to parallel vortical gust disturbances. Once again, none of those studies takes into account 3D effects, in particular those of wingtip vortexes, and are bound by the Reynolds numbers and reduced frequencies considered, which are far from the ones examined in this research. Here is where the interest for such a numerical study lies.

II. Details of the Computations

A. Configuration

Given that the ultimate goal is to use the simulations developed for the prediction of interesting phenomena to be experimented, the case configuration was determined by the experimental setup itself. Therefore, an unsteady 2D DNS of a NACA 0012 profile, with 1.5 cm of chord, at angle of attack $\alpha = 5°$, subject to a sinusoidal free-stream velocity following equation 1 was carried out.

$$U(t) = U_\infty(1 + \sigma sin(2\pi \frac{kU_\infty}{c} t + \varphi)) \tag{1}$$

$$k = \frac{fc}{U_\infty} \tag{2}$$

The simulation was calibrated taking mean velocity $U_\infty = 1$ m/s, surging amplitude $\sigma = 0.4$ and surging frequency $f = 2$ Hz. These values were chosen according to two criteria. The first one was to have a Reynolds number of $Re = 1000$, so that the computational costs associated with DNS were affordable. The second one was to keep the maximum similarity possible with the experimental case that was being studied in parallel at the DAEP. This experimental study assessed the flow over a NACA 0012, with 15 cm of chord, at $U_\infty = 10$ m/s and $f = 2$ Hz. Then, the similarity in Reynolds was not possible (the experimental one being $Re \sim 10^5$) but the reduced frequency similarity was. The reduced frequency (whose definition is 2) was $k = 0.03$ both in the experimental and the numerical case. In fact, the unsteady effects due to the oscillating wind are mainly dependent on k and σ, both of which were identical in the simulation and the experiments.

The domain was created and the boundary conditions (taking a velocity inlet and an atmospheric pressure outlet) were set in a suitable way, schematised in Figure 2.

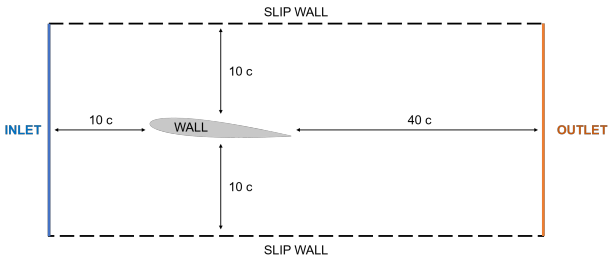

Fig. 2: Scheme of the location of the boundary conditions

According to DNS cell convergence criteria, in a small region around the aerofoil, the cell size was set to $\Delta x = c/100$ so that the cell Reynolds number was of $Re_{cell} = Re/100 = 10$. This is known to grant a sufficient resolution in order to capture the smaller turbulent scales. That region was 5 chords long and 2 chords wide, centred so the wake behind the profile could be apprehended. The mesh was further refined towards the leading and trailing edges, to adequately adapt to the curvature, and a limit growth factor of 1.15 was set throughout the domain. The resulting mesh can be seen in detail in Figure 3, having a number of cells of around 100'000.

The solver settings were the following, selected according to the flow physics studied:

- Laminar
- Implicit Unsteady
- Constant Density
- Segregated Flow
- Gas
- Two Dimensional

In order to choose the time-step for the unsteady solver, the two main characteristic times of the flow were considered: the surging inlet period and the convective time. Those were, respectively, $T = 1/f = 0.5$ s and $c/U_\infty = 1.5 \times 10^{-2}$ s. To capture both temporal scales, having 100 samples per characteristic time is typically sufficient. Being the smaller

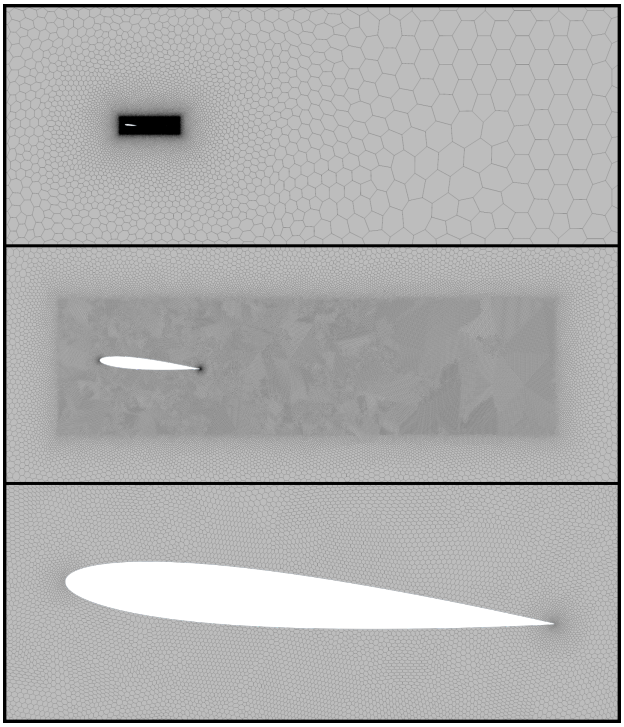

Fig. 3: 2D mesh with zoom-in around the refined region and the profile

time-scale the convective time and therefore more restrictive, it was selected giving a time-step of $\Delta t = 1.5 \times 10^{-2}/100 = 1.5 \times 10^{-4}$ s.

B. Mesh and time-step independence

To verify the simulation robustness, subsequent studies of mesh and time-step independence were carried out. For the mesh independence, the size of the cells in the refined domain was modified by a factor of 2, thus impacting the total number of cells by a factor of around 4. Characteristic parameters of the resulting sinusoidal lift and drag forces were calculated at each oscillating period - root-mean-square, mean, amplitude and period. Their variation along the number of periods was assessed to determine when the transient was purged and their variation between meshes was calculated to establish which mesh was independent for the study. The results are summarised in Figure 4. A clear transient state was identified to last 0.2 s, so the first period was discarded. Period nº 1 then designates the first period after the transient state.

All lift and drag parameters were observed to remain unchanged after the first period, thus after 1 s. Given that the time for a particle to cross the whole domain was $51c/U_\infty = 0.765$ s it was concluded that the transient had been evacuated. Therefore, all the subsequent simulations were run only for a duration of three periods in order to save computational time.

The evolution of the different parameters along meshes can be seen in Figure 5.

Concerning the lift, the mesh could be said to be independent at the base mesh of 100k cells, since the subsequent

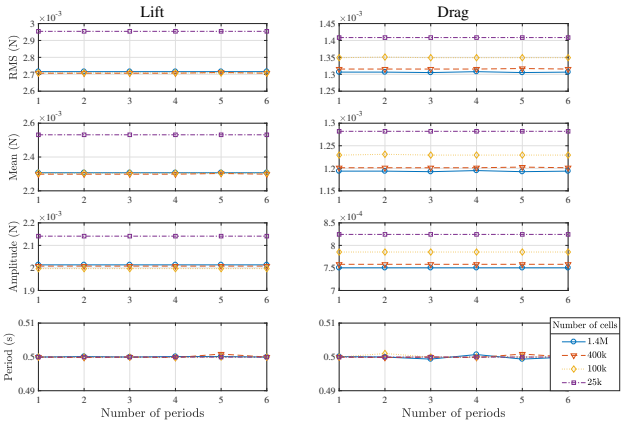

Fig. 4: Evolution of lift and drag parameters between periods for different meshes

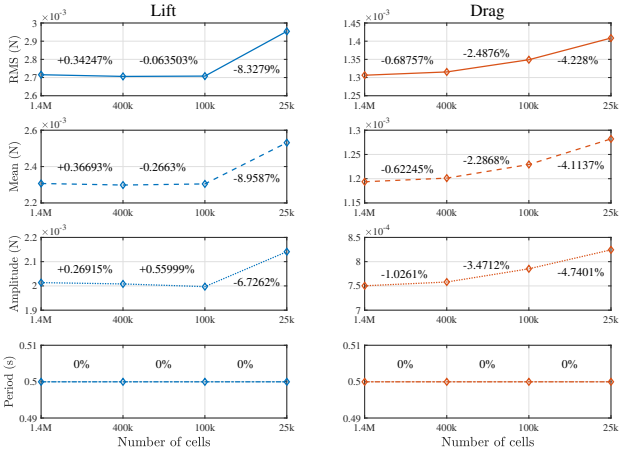

Fig. 5: Evolution of final lift and drag parameters between meshes

refinements only resulted in variations of under 1%. However, if considering the drag, a mesh of 400k cells would be needed to achieve independence following the 1% criteria. Nevertheless, given that drag is usually poorly predicted by CFD and that the magnitude of interest was the lift, the 100k-cells mesh was used throughout the simulations. This decision was taken to save computational cost, especially considering that a 3D simulation had to be created on the basis on the ones shown here.

Then, the time-step independence study was carried out. To do so, a factor of 2 was used again for the variation in the duration of the time-step and the main lift and drag parameters evolution was evaluated, as it can be seen in Figure 6.

It can be concluded that the results were unchanged even for a time-step 16 longer than the base one established, the variations of the parameters remaining under 0.5%. The base time-step of $\Delta t = 1.5 \times 10^{-4}$ s was kept in all the simulations for further precision, except for the cases with lower surging frequencies, since the computational times were then not reasonable.

The correct propagation without dissipation of the inlet

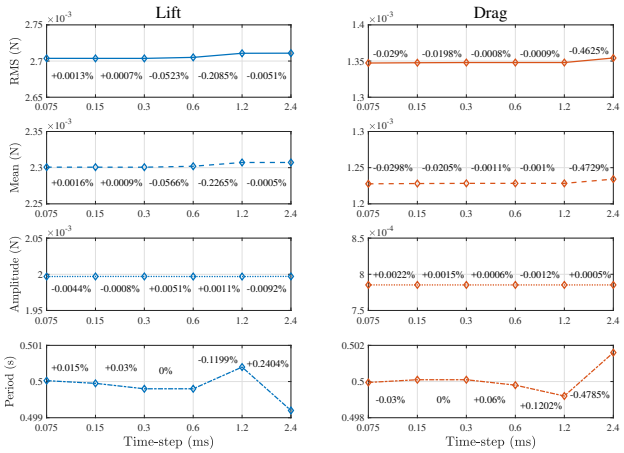

Fig. 6: Evolution of final lift and drag parameters between time-step durations

surging free-stream velocity along the fluid domain was also verified. This was done by removing the aerofoil from the domain while keeping the same mesh structure. Longitudinal velocity probes where placed as a 6x6 matrix through longitudinal and cross sections of the refined domain region and the recorded velocities are shown in Figure 7, together with the inlet surging velocity. It was verified that all the curves collapse and thus that the longitudinal velocity in the whole domain oscillates together without dissipation.

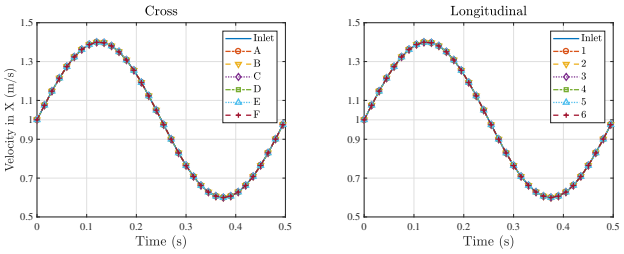

Fig. 7: Longitudinal velocity at different probes along cross and longitudinal sections of the refined domain region

III. Results

A. Low angle of attack laminar simulations

This section presents the results of all the laminar simulations with $\alpha = 5°$ and $\sigma = 0.4$, which is the main case of study which will also be experimented. The procedure for the assessment of the unsteady effects is the same independently of the other flow parameters selected in the different subsections. That is, firstly, the measurement of the unsteady lift produced in response to the surging inlet velocity. Secondly, the measurement of the steady lift resulting from steady simulations at discrete constant inlet velocities corresponding to the many values the unsteady sinusoidal inlet velocity takes along a surging period. Next, the fitting of those discrete steady lifts to an oscillating quasi-steady lift through a best-fitting smoothing spline. Lastly, the calculation of the unsteady-to-quasi-steady lift ratio along a surging period and the comparison to the theoretical solution predicted by Greenberg's Theory. This allows for the limits of Greenberg's Theory to be studied in the range of Reynolds numbers, reduced frequencies and surging amplitudes considered. Furthermore, knowing that - from the experimental measurements - at $Re = 10^5$ theoretical tendencies are followed, seeing if the unsteady effects obtained from the simulations and the theoretical ones match permits to conclude on whether or not low Re DNS allow to predict real high Re unsteady effects. Additionally, flow visualisation through vorticity magnitude contours and spectral analysis data are also presented in certain cases of interest for better understanding of the different physical phenomena.

1) Reynolds 1000: The unsteady effects at $Re = 1000$ are presented in Figure 8 for increasing reduced frequencies by a factor of 10. The corresponding theoretical solutions are shown in Figure 9.

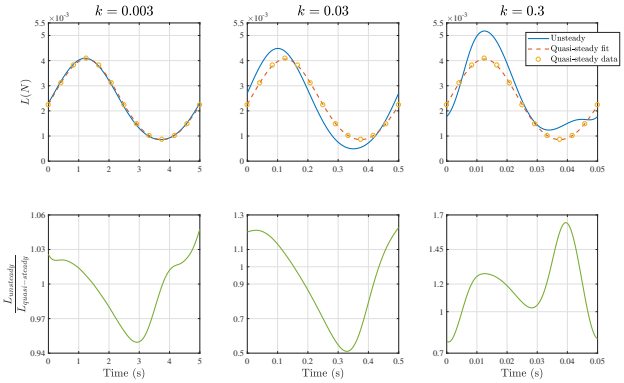

Fig. 8: Unsteady, quasi-steady lift and unsteady-to-quasi-steady lift ratio along a period for increasing reduced frequencies at $Re = 1000$

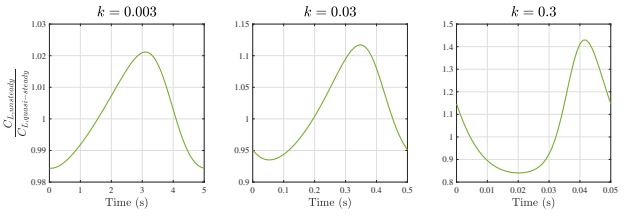

Fig. 9: Greenberg's Theory solution of unsteady-to-quasi-steady lift coefficient ratio along a period for increasing reduced frequencies

By looking at the unsteady and quasi-steady lifts, it is apparent that the separation between both increases with the reduced frequency. This is coherent since quasi-steady lift corresponds to an infinitely small reduced frequency - the reduced frequency being smaller the bigger the surging period with respect to the convective time. If considering the simulation unsteady-to-quasi-steady lift ratio, it appears clear that it does not follow the theory. Not only the maximum and minimum peaks deviate more from 1, but the evolution

tendencies are also reversed. The greater deviation could be exaggerated from the fact of having really low values of lift due to the small chord and speed, close to 0, which tends to increase the ratio. However, the opposed shape evolution makes it undeniable that the theory is not valid in this case. In fact, Greenberg predicts a lower unsteady lift with respect to the quasi-steady when accelerating, and a higher unsteady lift when decelerating (see Figure 9). This comes from the potential solution of the flow which implies constant circulation in the domain, with the variations in circulation in the wake due to the velocity oscillations inducing a variation in the effective angle of attack of the profile, thus acting as a "phase delay" in the unsteady lift evolution. This "delay" becomes more apparent the higher the reduced frequency. In the simulations, the unsteady lift is greater when accelerating and lower when decelerating. Since Greenberg's Theory is applied for inviscid flows at small surging amplitudes ($\sigma = 0.4$ taken here being close to the limit of validity) and regardless of the reduced frequency, this difference must arise from the Re. At such low Reynolds number, viscous effects are too dominant for the inviscid hypothesis to be applied and govern the unsteady behaviour. This is not the case in the experimental setup where, for a $Re = 10^5$ the advection being most influential, the boundary layer is thin enough so the general aerodynamic behaviour is piloted by the potential flow. Therefore it appears that such low Re DNS studies are unable to correctly predict the unsteady behaviour of higher Re flows. This main conclusion will be verified in many ways in the following sections.

Taking a closer look at the case $Re = 1000$, $k = 0.3$ an interesting phenomenon can be appreciated when the flow is accelerating. The unsteady lift does no longer follow a sinusoidal evolution. This is a sign of the flow being detached. This is evidenced in Figure 10, where the flow structure evolution in the boundary layer and the wake is shown. At $k = 0.3$, the accelerations in the flow become too great for the boundary layer to withstand. The local pressure gradient induced by the velocity variation creates a trailing-edge detachment as it appears in time instants 10c and 10d. Then, the detached boundary layer is pushed away as the flow reattaches (Figures 10e and 10a), shedding into two counter-rotating vortexes. The appearance of this vortex shedding at these particular Re and k conditions is very relevant, significantly affecting the aerodynamic behaviour of the profile. Predicting this phenomenon would be very complex or even impossible analytically, which makes these simulations data valuable for the characterisation of these flow conditions.

2) Experimental inlet velocity: For the experimental measurements, the surging inlet speed in the wind tunnel is achieved through the controlled opening and closing of valves at the outlet. Therefore, the inlet speed produced is not a perfect sinusoidal signal. The question of knowing if the difference in the shape of the inlet speed impacts the unsteady effects arises naturally, since Greenberg's Theory is only applied with perfect harmonic oscillations. To answer this question, the exact experimental inlet velocity was inputed in the simulations once re-scaled to keep a Re close to 1000. In Figure 11 the subsequent unsteady effects, results and the comparison with the theory are presented following the same procedure as for the ideal harmonic inlet speeds considered before. For the calculation of the approximate theoretical solution, the best fit of the experimental velocity to a sinusoidal function was found and its non dimensional parameters are shown in Figure 11, granting a Reynolds of around $Re \approx 864$. Once again, the obtained unsteady-to-quasi-steady lift ratio does not follow the theory, showing the same reverse behaviour as the perfect harmonic cases. The solution obtained is fairly close in shape and amplitude to the one of the base case of study with $Re = 1000$ and $k = 0.03$, which is not surprising since the inlet speeds are pretty similar. From this it can be concluded that the experimentally obtained shape of inlet velocity in the wind tunnel is such that its effects do not significantly differ from the ones a perfect harmonic speed would create.

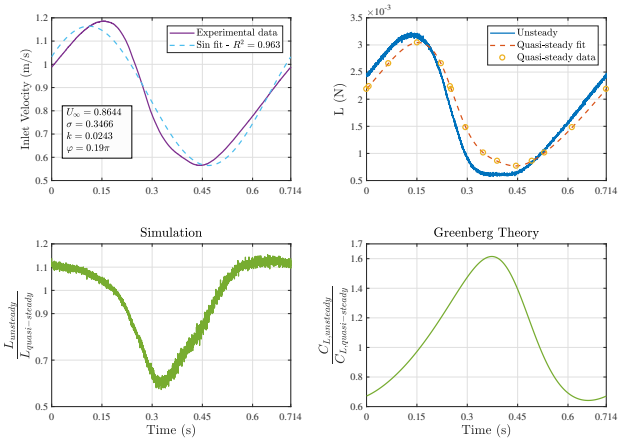

Fig. 11: Unsteady, quasi-steady lift and unsteady-to-quasi-steady lift ratio along a period for the experimentally measured quasi-sinusoidal inlet speed

3) Reynolds 100: Since the results for $Re = 1000$ lead to concluding that it is the viscosity effects that dominate and make the unsteady response deviate from the theory, it would be normal to expect the resemblance of the real and theoretical unsteady-to-quasi-steady lift ratios to be piloted by the Reynolds number. Therefore the impact of Re on the unsteady effects was to be evaluated.

At $Re = 100$ the mesh is fine enough to capture all the turbulent scales. The flow being even more viscous, a viscous-dominated unsteady response is expected. That is, in fact, what can be found in Figure 12. Overall, unsteady lift appears less different from quasi-steady, the viscosity attenuating the unsteady effects. Still, Greenberg predicted solutions are clearly not followed for $k = 0.003$ and $k = 0.03$. However, for $k = 0.3$, the unsteady-to-quasi-steady lift ratio appears similar to the one predicted by the theory. Despite that, a clear cause can not be stated since small changes in a

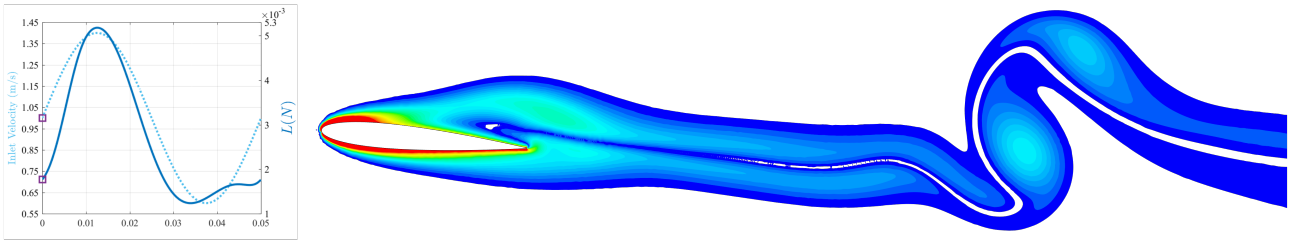

(a) $t = 0$

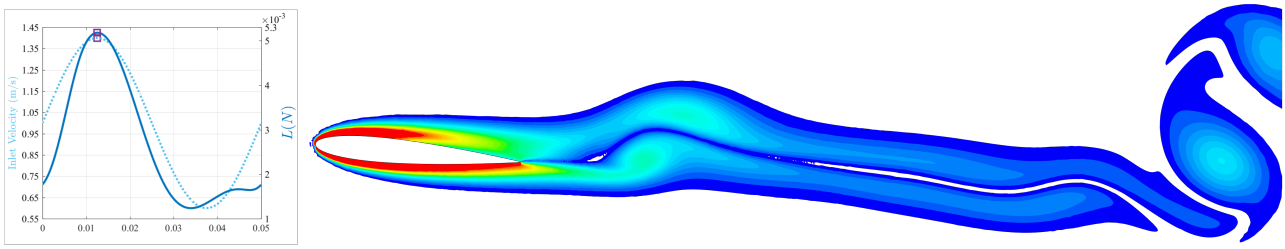

(b) $t = T/4$

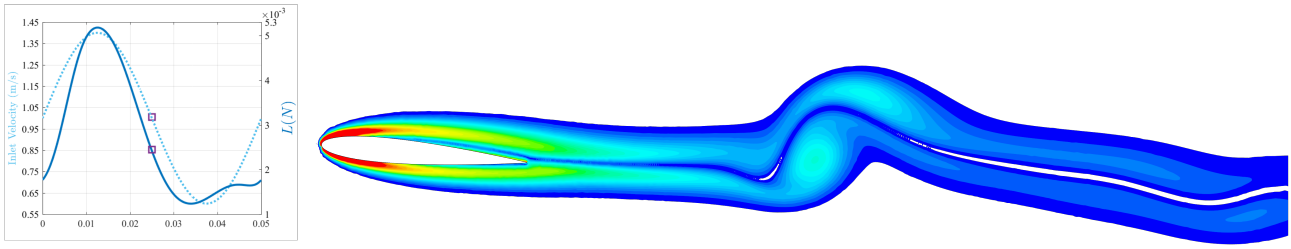

(c) $t = T/2$

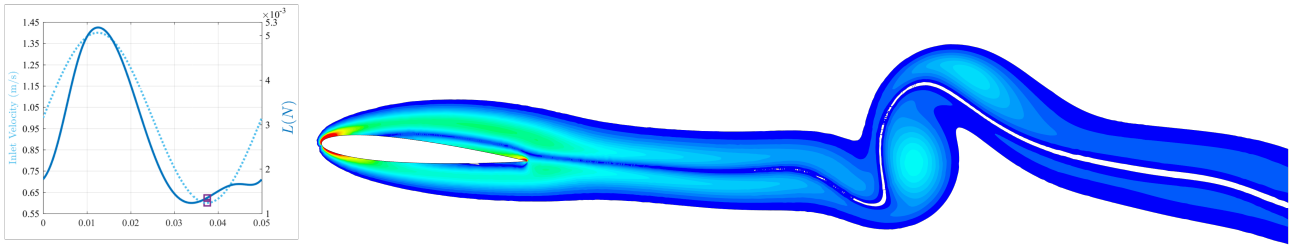

(d) $t = \frac{3}{4}T$

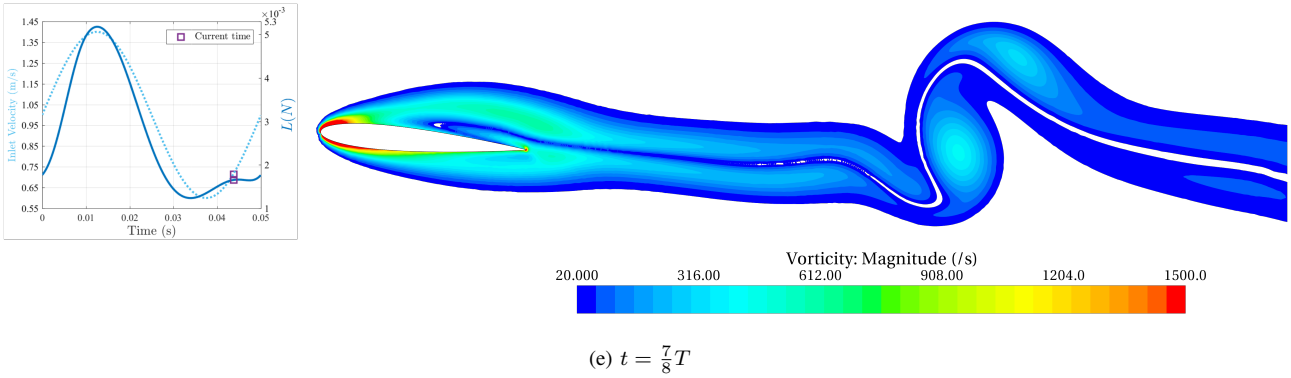

(e) $t = \frac{7}{8}T$

Fig. 10: Evolution along a period of the vorticity magnitude contours in the aerofoil wake for $k = 0.3$ and at $Re = 1000$

fairly complex flow such as this one can have a great impact on different phenomena. The solutions shown here are the result of many overlapping phenomena, further work would be required to properly isolate them and assess the complete flow mechanics.

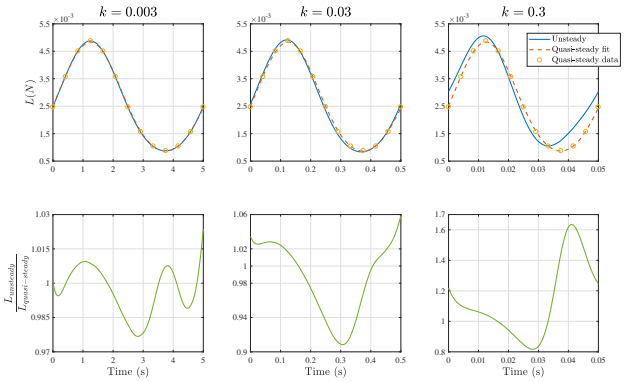

Fig. 12: Unsteady, quasi-steady lift and unsteady-to-quasi-steady lift ratio along a period for increasing reduced frequencies at $Re = 100$

4) Reynolds 10'000: Due to the decrease in the smaller turbulent scales' size, the mesh is not fine enough for a $Re = 10'000$, resulting in an under-resolved flow. Even so, the unsteady effects were calculated, as an approximation, with the aim of assessing their variation with Re. The resulting flows can be observed in Figure 13, in which, no matter k, the wake is destabilised and trailing-edge vortex shedding appears. In fact, at $Re = 10'000$ and $\alpha = 5°$ vortex shedding is present even for steady constant velocity flows. This phenomena appears for an α between 3°and 4°as proven in Figure 14. This destabilisation of the wake is related to the flow building up turbulence. However, without a further mesh independence study at $Re = 10'000$, it is not possible to determine whether this turbulence is natural to the flow or comes from numerical dissipation due to the mesh under-resolution.

The unsteady-to-quasi-steady lift (Figure 15) ratios were obtained by taking the mean value of the oscillating lift for the quasi-steady constant velocity cases. Since vortex shedding occurs, one of the main hypothesis of Greenberg's Theory is not respected. It is only normal that the results do not follow the theory. Additionally, the lift oscillations coming from the vortex shedding combined with the low lift values result in exaggerated lift ratio peaks that render the unsteady effects assessment not feasible with the methods applied.

It is interesting to point out how the vortex shedding appears to have a distinct frequency (see Figures 13a and 13b) independent from k, which mixes with the main oscillation of lift once the reduced frequency reaches $k = 0.3$ as in 13c. This derives in a complex wake structure. A very rough approximation of the apparent vortex shedding frequency provides a value of around $f_{VS} \approx 180$ Hz. If the Strouhal number is calculated taking the maximum thickness of the profile as characteristic length the result is $St = f_{VS} 12\% c / U_\infty \approx 0.324$, which is

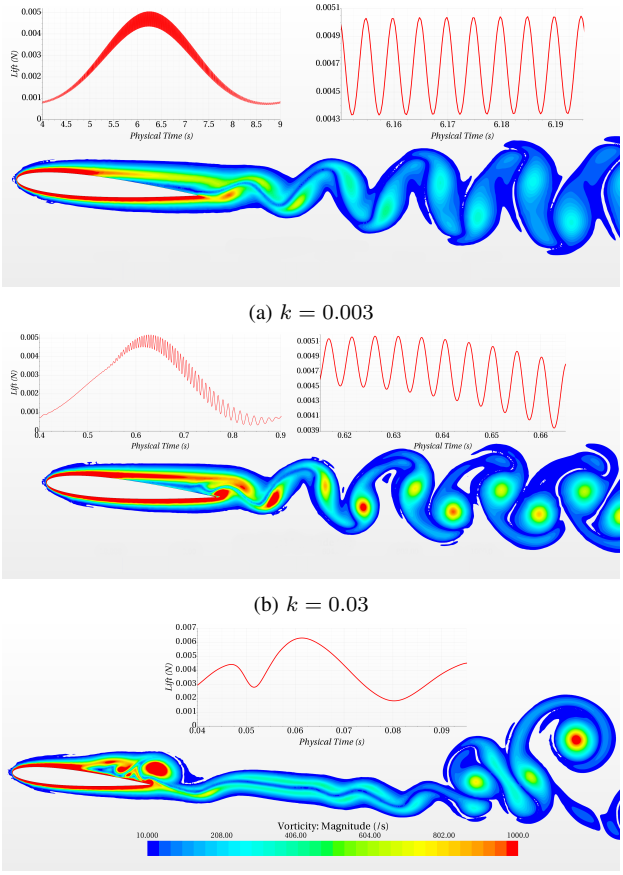

(a) $k = 0.003$

(b) $k = 0.03$

(c) $k = 0.3$

Fig. 13: Lift and vorticity magnitude contours in the aerofoil wake at $Re = 10000$ for different reduced frequencies

close to typical St values found in literature. These results would require more in depth and consistent analysis but still provide a general idea of the physics found.

Since vortex shedding phenomena is present, spectral analysis was performed on the lift to provide complementary data for future research and is shown in Figure 16. The main surging frequency is very apparent independently from the case taken. While for $Re = 100$ and $Re = 1000$ there are no other frequencies present (except for the harmonics in the case of $Re = 1000$ and $k = 0.3$ where the detachment appears), for $Re = 10'000$ a very rich spectral content is present, with lower amplitude higher frequencies appearing. Yet, no clear predominant secondary peak due to the vortex shedding appears, the previously estimated $f_{VS} \approx 180$ Hz, being surrounded by what resembles noise, which is unexpected. For $Re = 10'000$ and $k = 0.3$ all the harmonic frequencies associated to the main surging one are shown clearly and distinctly. Once again the physics at $Re = 10'000$ would need further research that is out of the scope of this project.

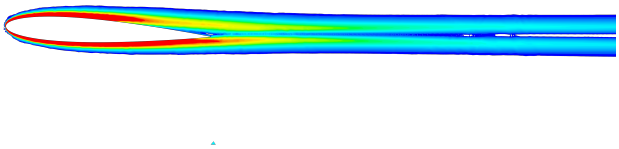

(a) $\alpha = 3°$

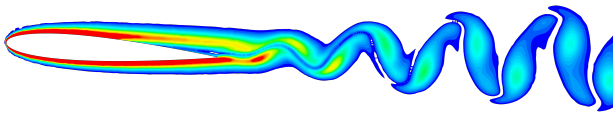

(b) $\alpha = 4°$

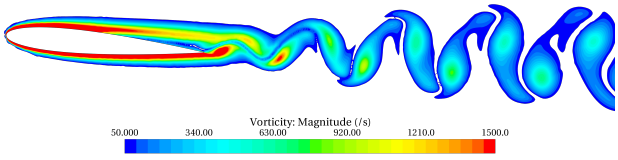

(c) $\alpha = 5°$

Fig. 14: Vorticity magnitude contours in the aerofoil wake at $Re = 10000$ with constant inlet velocity of 1 m/s for different angles of attack

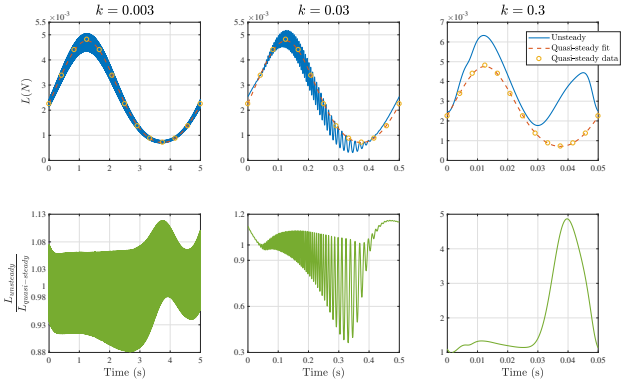

Fig. 15: Unsteady, quasi-steady lift and unsteady-to-quasi-steady lift ratio along a period for increasing reduced frequencies at $Re = 10000$

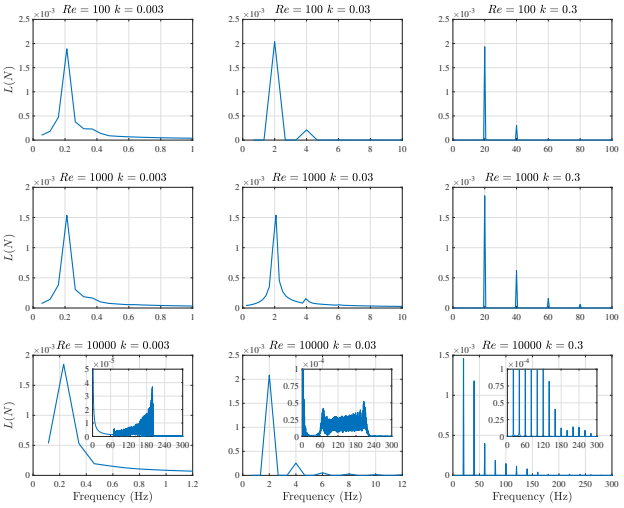

Fig. 16: Sigle-sided lift amplitude spectra for different reduced frequencies and Reynolds numbers

B. Low angle of attack inviscid simulations

To finally confirm the predominant role of viscosity in the unsteady effects observed, results of inviscid simulations for $\alpha = 5°$ and different values of k and σ are presented here. The goal is to set the flow conditions such that all Greenberg's Theory hypothesis are fulfilled in order to validate the simulations and the conclusions reached. The unsteady-to-quasi-steady lift ratios are calculated and compared to the theory for increasing reduced frequencies (Figure 17) and for increasing surging amplitudes (Figure 18).

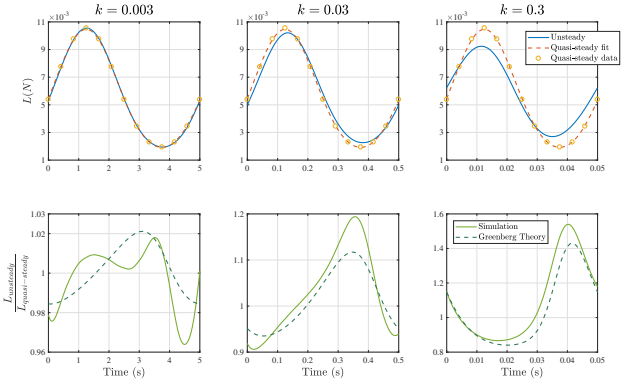

Fig. 17: Unsteady, quasi-steady lift and unsteady-to-quasi-steady lift ratio along a period for increasing reduced frequencies in the inviscid case - $\sigma = 0.4$

As it can clearly be seen, the results obtained follow Greenberg's Theory as expected with very little differences - the most distant case being the low frequency $k = 0.003$, being almost quasi-steady. The increase in k further deforms the curve increasing the apparent "time delay" (as evidenced in Figure 9) and the increase in σ only impacts the amplitude, not the shape (as shown in Figure 19).This proves that the simulations are valid and that the viscosity is definitely the

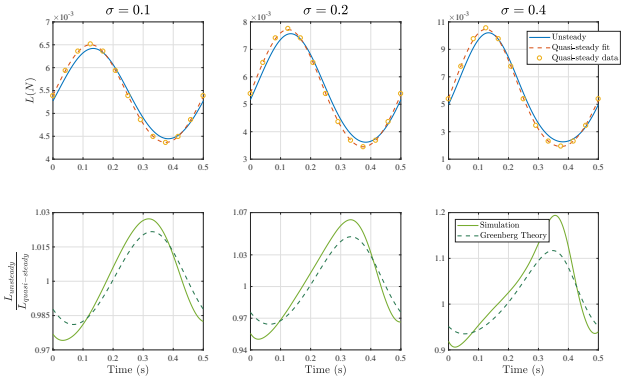

Fig. 18: Unsteady, quasi-steady lift and unsteady-to-quasi-steady lift ratio along a period for increasing surging amplitudes in the inviscid case - $k = 0.03$

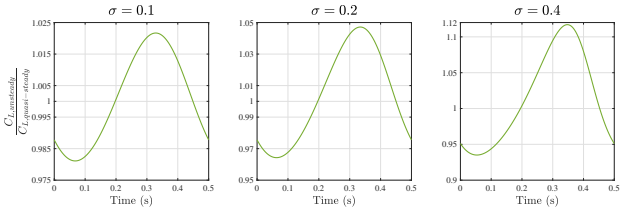

Fig. 19: Greenberg's Theory solution of unsteady-to-quasi-steady lift coefficient ratio along a period for increasing surging amplitudes

source of the discrepancies at low Reynolds numbers.

Finally, in order to understand how viscosity impacts the lift locally, the pressure coefficients are used. Pressure coefficient for unsteady and steady inlet velocities are compared at characteristic time instants both in the viscous and the inviscid cases for the main $Re = 1000$, $k = 0.03$ and $\sigma = 0.4$ scenario in Figure 20. General unsteady effects can be found in both the viscous and the inviscid case. When the flow accelerates (Fig.20a) the pressure at the trailing edge is lower in the unsteady case, higher when it decelerates (Fig. 20c), and the same if there is no acceleration (Figs. 20b and 20d). Even with this common phenomena independent from viscosity, due to the pressure gradients induced by the velocity fluctuations, the viscous and non viscous unsteady-to-quasi-steady lift ratios show opposed tendencies. This is due to the fact that different mechanisms pilot the unsteady behaviour in each case. In the inviscid case, it is a higher or smaller depression at the leading edge that essentially determines if the lift is higher or lower in the unsteady case. This comes from the induced effective angle of attack variation created from the potential flow. On the other hand, in the viscous case, thick boundary layers develop along the profile and govern its aerodynamics. No local effect is observed, but a general impact on the suction and pressure surfaces appears instead. It is the whole boundary layer, mainly the one on the suction side that is responsible for the unsteady effects. This is especially visible when the flow decelerates and reaches minimum velocity (Fig. 20d), with the unsteady lift reaching its minimum and the unsteadiness being more important. As a general explanation, it can be said that the thickened boundary layer has trouble absorbing the velocity variations associated with the surging flow. Most importantly during the deceleration and for a higher reduced frequency, even provoking its detachment as seen previously in Figure 10.

C. High angle of attack simulation

At low Re and α the unsteady effects cannot be compared to the experimental ones due to Reynolds effects. However, it is known that for a fully separated flow, the turbulent structures developed are independent of Re. Thus, in order to be able to later compare the simulations with the experiments, a high angle of attack $\alpha = 20°$ case was simulated using a further refined mesh to fully capture all the wake content. The flow structure evolution and spectral analysis are shown in Figures 21 and 22, respectively. The main surging frequency is still present, but amplitude oscillations appear related with the wide flow separation. The formation of counter-rotating leading-edge and trailing-edge vortexes can be observed, with a main associated frequency in between 40 Hz and 50 Hz. If further experimental research at high angles of attack takes place, the low Re DNS should be able to fully predict the experimental flow structure. In that case, this data would be the starting point for comparison and validation.

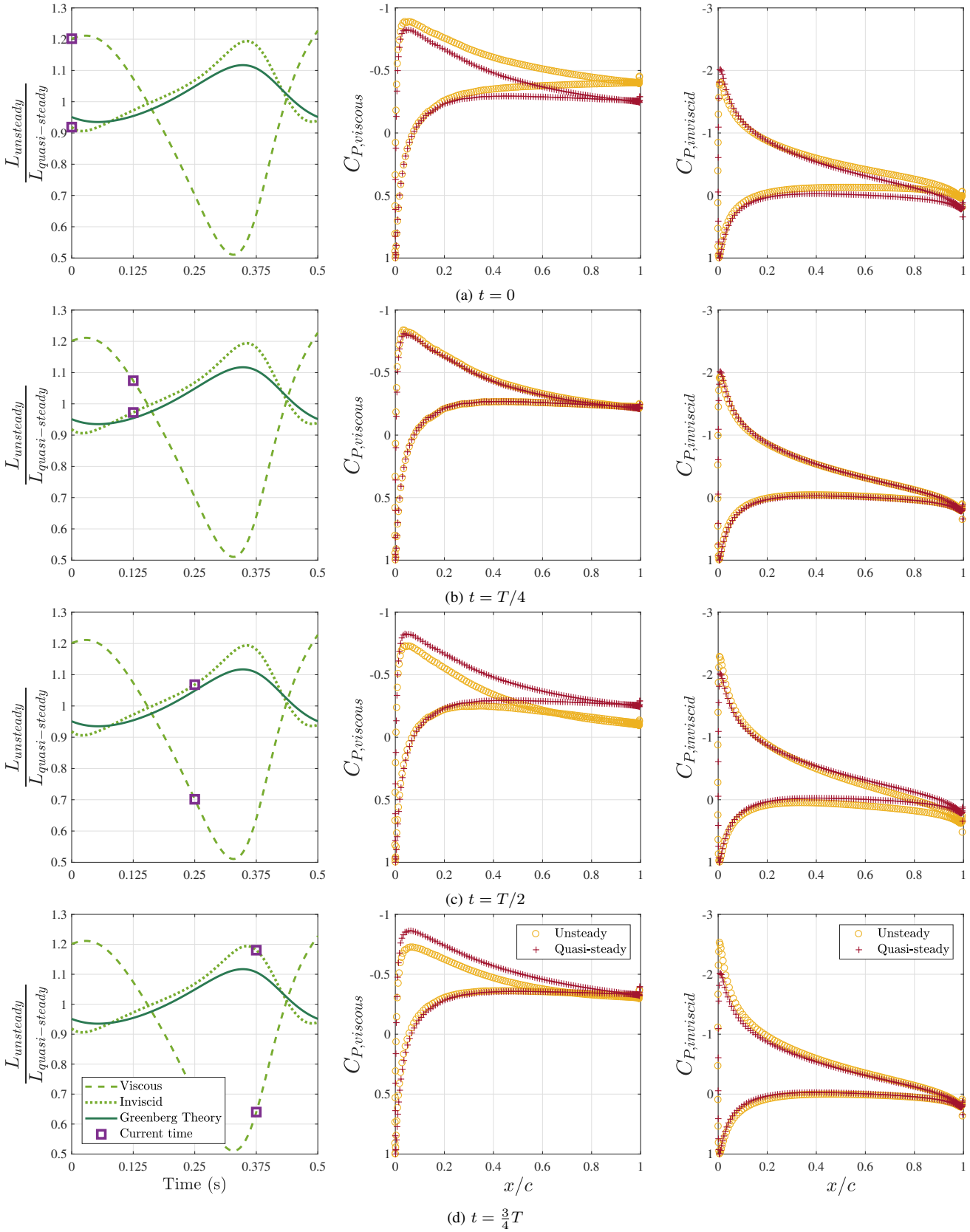

(a) $t = 0$

(b) $t = T/4$

(c) $t = T/2$

(d) $t = \frac{3}{4}T$

Fig. 20: Evolution along a period of the pressure coefficient in the viscous ($Re = 1000$) and inviscid cases at $k = 0.03$ and $\sigma = 0.4$ with comparison between the unsteady and the quasi-steady simulation solutions for each case

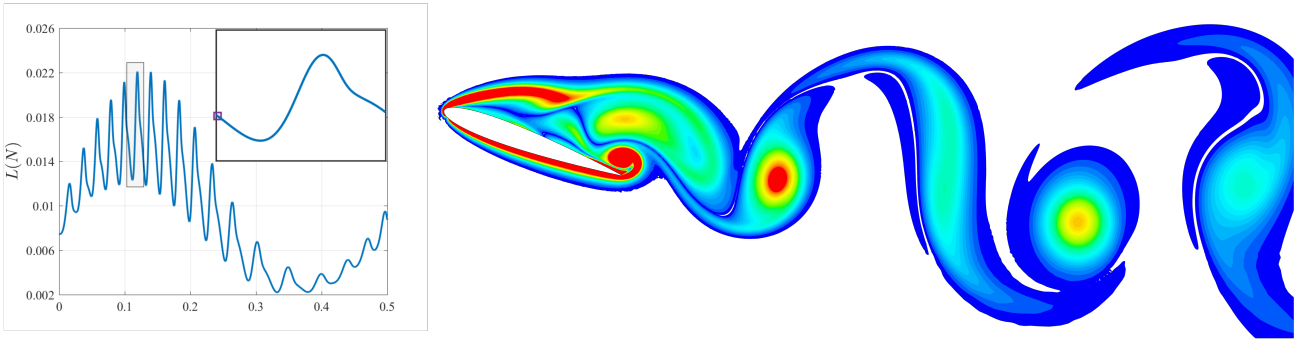

(a) $Mean$

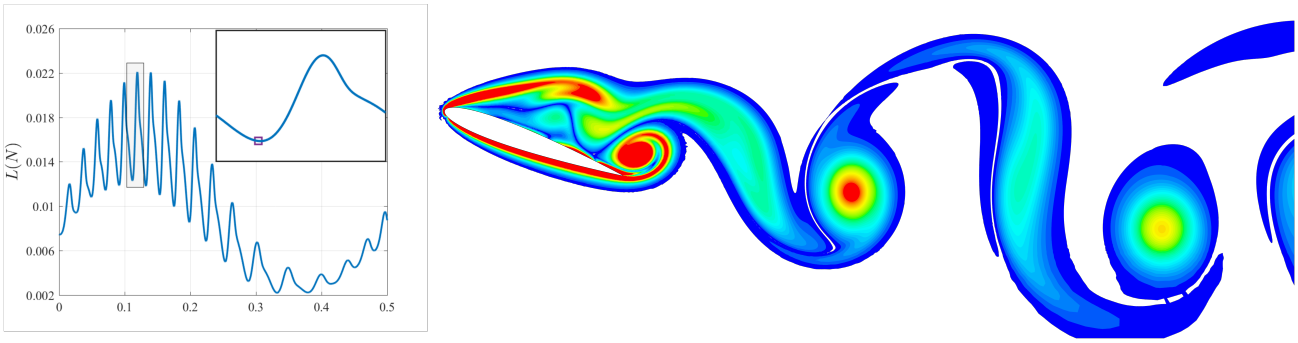

(b) $Minimum$

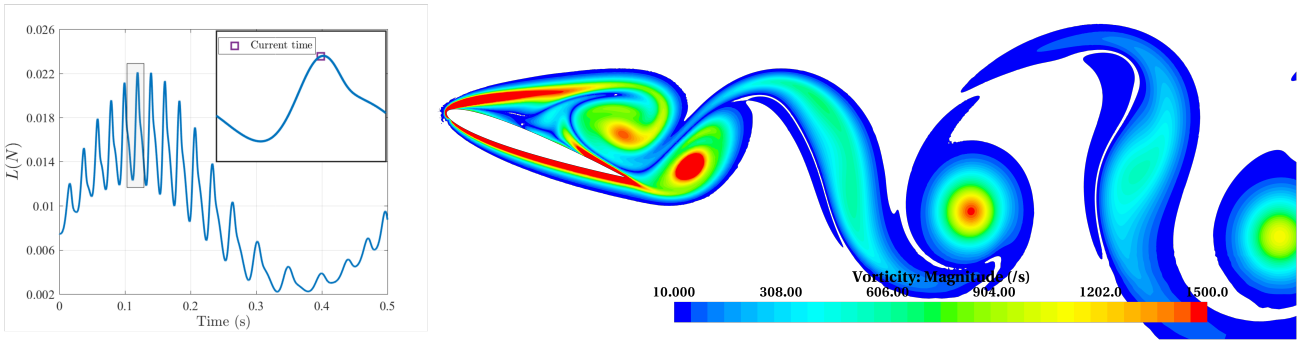

(c) $Maximum$

Fig. 21: Evolution along a lift oscillation of the vorticity magnitude contours for $k = 0.3$, $\sigma = 0.4$ at $Re = 1000$ and $\alpha = 20°$ - Formation of the leading and trailing-edge vortexes

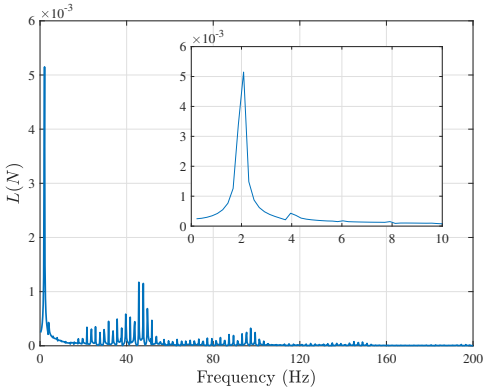

Fig. 22: Sigle-sided lift amplitude spectra for the 20º angle of attack case

IV. Conclusion and Future Work

This researche focused on the study of the unsteady effects present in a surging velocity flow over a NACA 0012 profile at low Re, σ, k and α through two-dimensional DNS. The aim was to determine whether or not these simulations' results could be extrapolated to real micro-drone flight conditions, at higher Re where Greenberg's Theory predictions are valid. It was found that at such low Reynolds numbers and angles of attack, viscous effects dominate the unsteady response, showing an opposed behaviour to the theoretical one. It is the global interaction of the profile's thick boundary layer with the surging velocity that pilots the lift. The boundary layer shows to be sensitive to the surging-induced pressure gradients especially with decelerating flow at higher reduced

frequencies.

The evolution of the unsteady behaviour with Re could be further studied. One could even imagine a complete characterisation of the unsteady response of the NACA 0012 profile in function of the main flow parameters: Re, σ, k and α. However a DNS approach might be too costly, especially for higher Re, LES or RANS simulations being perhaps more suitable. Approximate results that could be used as validation tools and starting points for the mentioned future research are presented in this paper.

A three-dimensional simulation of this case was created but its results could not be utilised due to computational cost and time constraints. The next step for this project is to move to the 3D case and to study the new implications that the fact of having a finite wing brings in relation to the unsteady behaviour. Even though the 3D low Re DNS will not be able to predict the real high Re lift behaviour, perhaps it will give relevant information on how the wind tip vortex interacts with the surging velocity.

REFERENCES

[1] Caleb J. Barnes and Miguel R. Visbal. Further investigations of vortical gust/airfoil interactions at a transitional reynolds number. In *2018 AIAA Aerospace Sciences Meeting*. American Institute of Aeronautics and Astronautics, Jan 2018.

[2] Caleb J. Barnes and Miguel R. Visbal. Gust response of rigid and elastically mounted airfoils at a transitional reynolds number. *Aerospace Science and Technology*, 74:112–119, Mar 2018.

[3] NASA Langley Research Center. *Wake Vortex Study at Wallops Island*. May 1990.

[4] J. M. Greenberg. Airfoil in sinusoidal motion in a pulsating stream. In *NACA Tech. Rep.TN1326.*, Jun 1947.

[5] C. Strangfeld, H. Müller-Vahl, C. N. Nayeri, C. O. Paschereit, and D. Greenblatt. Airfoil in a high amplitude oscillating stream. *Journal of Fluid Mechanics*, 793:79–108, Mar 2016.

[6] Simon Watkins, Juliette Milbank, Benjamin J. Loxton, and William H. Melbourne. Atmospheric winds and their implications for microair vehicles. *AIAA Journal*, 44(11):2591–2600, Nov 2006.